The Photophysical Properties of 6-Azaindole

Susan M. Twine,[§] Lise Murphy,[§] Robert S. Phillips,[‡] Patrik Callis,[†] Michael T. Cash,[‡] and Arthur G. Szabo*[,§]

Department of Chemistry, Wilfrid Laurier University, 75 University Ave., Waterloo, Ontario N2L 3C5, Canada, Departments of Chemistry and of Biochemistry and Molecular Biology, University of Georgia, Athens, Georgia 30602, and Department of Chemistry and Biochemistry, Montana State University, 108 Gaines Hall, Bozeman, Montana 59717

Received: September 30, 2002; In Final Form: October 24, 2002

The biosynthetic incorporation of tryptophan analogues into proteins using plasmid expression systems has been shown to offer advantages in fluorescence spectroscopic studies of the molecular details of the interacting segments of protein−protein complexes. There are two underlying concepts of this approach. The first is based on a close structural similarity between the analogue and the native tryptophan. The second is that the analogue has an extended red absorbance permitting the selective excitation in the presence of tryptophan. The reported intense absorbance band of 6-azatryptophan at 325 nm would appear to offer a unique opportunity of using this analogue in such studies. In this work, we present the photophysical characterization of the excited state behavior of 6-azatryptophan through a complete study of the cognate indole moiety, 6-azaindole. It was found that the absorbance at 320 nm for 6-azaindole and 325 nm for 6-azatryptophan was due to the protonated form in which both ring nitrogens are protonated. The protonation equilibrium for 6-azaindole had a pK_a value of 8. The fluorescence of 6-azaindole was centered at 380 nm. It was found that the neutral form of 6-azaindole was nonfluorescent in nonpolar solvents. In aqueous solution at pH values between 6.5 and 10, the fluorescence maximum of 6-azaindole remained at 380 nm, and the intensity decreased as the pH increased. Above pH 10, there was increased fluorescence on the low-energy side of the spectrum until at pH 14 the fluorescence spectrum showed a single maximum at 440 nm. The observations of the collective experiments in a variety of solvent conditions and pH values, including time-resolved fluorescence measurements, permitted a consistent assignment of each of the fluorescence species together with a rationalization of the excited-state processes that result from the excitation of either the protonated form or the neutral N1−H tautomer. The 440 nm fluorescence was attributed to the fluorescence from the excited state of the N6−H tautomer, a species that formed from the protonated excited state molecule that had previously been formed from initial excitation of the N1−H ground state. The work reports determinations of the excited-state pK_a values of each of the three species. The relative energy values of each of the ground-state molecules and excited-state species could be estimated. The relevance of the photophysics of 6-azaindole to protein structural studies was demonstrated by the biosynthetic incorporation of 6-azatryptophan into the Y99W mutant of rat calmodulin and the observation of 6-azaindole fluorescence from this protein.

Introduction

Tryptophan fluorescence has been used extensively to study segmental flexibility, protein structure−function relationships, and protein interactions.[1,2] The choice of tryptophan is based on several factors. Often, there are limited numbers of tryptophan residues in proteins. Tryptophan has a moderately high molar extinction coefficient and an absorption spectrum that extends beyond the other aromatic amino acids, tyrosine and phenylalanine; therefore, its fluorescence can be preferentially excited in proteins. As a consequence of the excited-state electronic properties of the indole moiety, the fluorescence behavior of tryptophan is highly dependent on its environment, degree of exposure to solvent, and local dipole effects and thus provides a high level of information content on protein segmental structure and dynamics.[3]

With the advent of site-directed mutagenesis, one can effectively use tryptophan fluorescence to study multitryptophan-containing proteins by reducing the number of tryptophan residues to a single occurrence. In this way, one can obtain information that can be specifically attributed to a single residue. The study of protein−protein interactions by fluorescence spectroscopy is limited if both proteins contain tryptophan residues. A specific tryptophan residue cannot be selectively excited, and the relationship between the fluorescence and structural details becomes difficult to interpret. For this reason, analogues of tryptophan having extended red absorbancies have been investigated and biosynthetically incorporated into proteins in place of tryptophan.[4−7] In these cases, it is then possible to selectively excite the fluorescence of the tryptophan analogue in the presence of natural tryptophan at a wavelength in its extended absorption spectrum at which native tryptophan has negligible absorbance. For example, tryptophan analogues such as 5-hydroxytryptophan (5HW) and 7-azatryptophan (7AW) have extended red absorbancies that allow selective excitation of their fluorescence at wavelengths up to 315 nm. The advantages of using such intrinsic fluorophore analogues over labeling a protein with an extrinsic probe have been reviewed.[8]

One tryptophan analogue, 6-azatryptophan (6AW) (Figure 1), was shown to have a well-defined absorbance band centered at

* To whom correspondence should be addressed. E-mail: aszabo@wlu.ca. Tel.: 519-884-0710 ext. 2129. Fax: 519-884-0464.
[§] Wilfrid Laurier University.
[‡] University of Georgia.
[†] Montana State University.

10.1021/jp027102r CCC: $25.00
Published on Web 12/17/2002

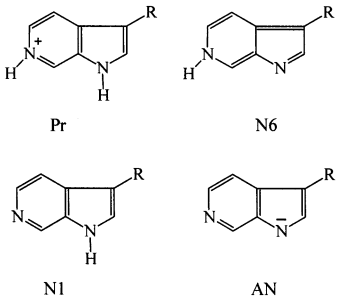

Figure 1. 6-Azatryptophan and 6-azaindole structures. Pr refers to the form protonated at N_1 and N_6, N1 to the form protonated on N_1, N6 to the neutral tautomer having hydrogen on N_6, and AN to the anionic form. R = H for 6-azaindole, and R = $^{+}H_3N-CH-COO^{-}$ for 6-azatryptophan.

325 nm and a high molar extinction coefficient of 9800 M^{-1} cm^{-1} in aqueous solution at neutral pH values.[9] However, there was no evidence that its fluorescence properties had been rigorously investigated. The well-defined absorption spectral band of 6AW would offer special advantages for selective excitation in the presence of natural tryptophan in protein−protein complexes. However, there are two factors that are required before such a utility can be realized. The photophysical properties of 6AW must be characterized to allow the interpretation of fluorescence data from proteins containing it. Equally important, the biosynthetic incorporation of 6AW into proteins must be demonstrated. In this report, we present a complete elucidation of the interesting photophysical properties of the core 6-azaindole (6AI) moiety. In addition, we show that it can be biosynthetically incorporated into a single tryptophan mutant of rat calmodulin (CaM).

Materials and Methods

Sample Preparation. 6AI and 6AW were synthesized as described previously.[9] Organic solvents were spectral grade (EM Science). Unless otherwise stated, all other materials were obtained from Sigma-Aldrich or VWR.

Solutions of 6AI and 6AW were prepared in buffers appropriate to the experiment normally at a concentration of 2.5 μM. Buffer solutions were 10 mM sodium phosphate, tris(hydroxymethylaminomethane) (TRIS), or piperizine-*N*,*N*′-bis[2-ethanesulfonic acid] (PIPES) adjusted to the appropriate pH. Acetonitrile−water and methanol−water mixtures were prepared on a volume per volume (v/v) basis. For cases in which these solvent mixtures were at different pH values, the pH of the aqueous component was first prepared, followed by the addition of the organic solvent to the appropriate percentage, and then the pH was readjusted to the nominal pH as necessary.

Steady-State Fluorescence Spectra. Fluorescence spectra (20 °C) were recorded on a Cary Eclipse spectrofluorimeter with excitation and emission band-pass of 5 nm and a path length of 0.5 or 1 cm. Fluorescence spectra of protein solutions were recorded in 10 mM buffer with 100 mM NaCl. All spectra were uncorrected for instrument sensitivity. A solution blank was subtracted from each spectrum. Absorbance spectra of these solutions were recorded using a Cary 50 UV−vis spectrophotometer with a path length of either 1 or 5 cm. Difference fluorescence spectra were calculated in some cases after the pair of spectra were normalized. The normalization procedure involved one of two methods. In some instances, the spectra were simply normalized to have the same value at one of the spectral maxima. Then, one of these normalized spectra was subtracted from the other. The other method used involved calculating the ratio of fluorescence intensities at a set of wavelengths on the high-energy side of the spectrum that had the maximum with highest energy. These ratios were averaged and used to normalize the two spectra over this wavelength range. Then, one spectrum was subtracted from the other.

Biosynthetic Incorporation of 6AW into a Single-Tryptophan Mutant of Calmodulin. 6AW was biosynthetically incorporated into a mutant of rat calmodulin (CaM) into which a single tryptophan residue had been inserted in place of tyrosine at position 99 (denoted Y99W mutant). The biosynthetic incorporation of 6AW into the Y99W mutant of CaM was carried out using the auxotrophic *E. coli* strain W3310 TrpA88,[10] which is deficient in the ability to produce tryptophan. Cells must be supplemented with an external source of tryptophan to sustain cell growth. In this manner, the level of external tryptophan may be controlled and limited. Cells may then be supplemented with the appropriate tryptophan analogue, which is then incorporated into proteins in place of tryptophan.

The cell line was transformed with the plasmid pKK223-3 (Pharmacia) containing the gene for the rat CaM mutant Y99W. Cells were grown in LB media for 22 h at 37 °C with vigorous shaking to an OD_{600} of greater than 1. The cells were then harvested, and the pellets were washed in minimal media to remove traces of tryptophan. Cultures were then resuspended in 25% of the original volume in M9 minimal media[11] enriched with 40% glycerol. 6AW was added to a total of 20 μg/L, and the cultures were incubated at 37 °C for a further 30 min. The expression of CaM Y99W was then induced by the addition of IPTG (Melford, U.K.) to a final concentration of 1 mM. At 5 h post-induction, the cells were harvested.

The mutant protein Y99(6AW) was purified as described previously[12] with the following modification. The gel filtration step was not included, but the protein was cleared of high molecular weight impurities using centrifugal filter devices (Millipore) with a 30 000 kDa MW cutoff. After purification, the protein was analyzed using SDS−PAGE gel and appeared as a single band with no detectable impurities.

Time-Resolved Fluorescence Measurements. Fluorescence intensity decay measurements were performed by the method of time-correlated single-photon counting (TCSPC).[13] Samples were excited by picosecond pulses of ultraviolet light generated by a frequency-doubled diode-pumped YAG laser (Coherent 9200 V-10), mode-locked at 76 MHz operating at 532 nm, that in turn pumped a Ti:sapphire laser (Coherent Mira 900) tuned to 927 nm. A pulse picker reduced the laser repetition rate to 4.8 MHz. The light then passed through a frequency tripler (Inrad 5-050) to generate 302 nm pulses for excitation. The sample emission passed through a polarizer oriented at 55° (magic angle). Fluorescence was detected after passing through a monochromator with a band-pass of 10 nm by a microchannel plate photomultiplier tube (Hamamatsu R2809U-06). The instrument response function (IRF) was collected using light scattered by a dilute suspension of colloidal silica. The sample chamber, collection optics, and timing electronics are described elsewhere.[14] Fluorescence decay curves were collected into 2000 channels of a multichannel analyzer with timing calibration of 20 ps/channel. Three curves were collected, the instrument response function, the sample fluorescence decay curve, and the solvent blank curve. The solvent blank curve was subtracted from the sample decay curve prior to data analysis.

Time-resolved fluorescence data were analyzed by standard reconvolution procedures described previously.[15,16] The fluorescence intensity decay was fit to a sum of exponentials:

$$I(t) = \sum \alpha_i \, e^{-t/\tau_i}$$

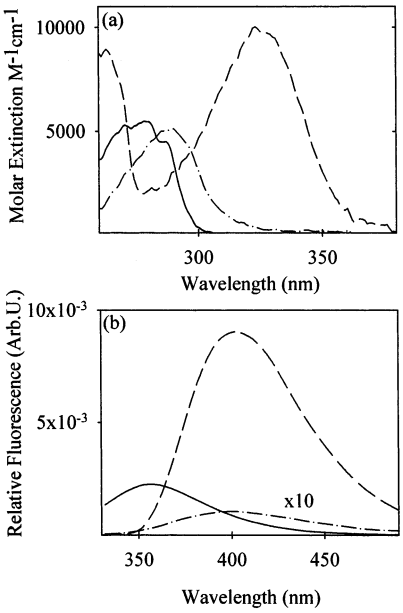

Figure 2. Absorbance and fluorescence emission spectra of tryptophan, 7-azatryptophan, and 6-azatryptophan: (a) absorbance spectra and (b) fluorescence spectra of 2.5 μM solutions of each of tryptophan (—), 7-azatryptophan (—·—) and 6-azatryptophan (— — —) in 10 mM phosphate buffer, pH 7.4. Excitation wavelengths were 295, 310, and 308 nm for tryptophan, 7-azatryptophan, and 6-azatryptophan, respectively.

where the preexponential terms, α_i, are the amplitudes and τ_i are the fluorescence decay times of each component. Global analysis procedures were performed with τ_i as the common parameters.[17,18]

Quantum Chemical Computations. Ab initio quantum chemical computations were carried out with Gaussian 98 (revision A.6).[19] Two sets of calculations were carried out, one with the 3-21G basis and one with the 6-31+G** basis. Ground-state energies are geometry-optimized Hartree−Fock values. Excited-state energies are geometry-optimized CIS (Configurational Interaction using Singlet excited state configurations) values. In addition, ground-state energies were also obtained by optimizing geometry at the MP2/6-31+G** level. This level of calculation has been reported to estimate proton affinities of nucleic acid bases to within 2% accuracy.[20] A similar study on the tautomerization of 7-azaindole[21] correctly predicted the reversal of energy ordering of the tautomers in the excited state. In that study, inclusion of solvation energy by the self-consistent reaction field method was found to change the relative energies of the two tautomers by 1.8 kcal/mol.

Results

The objective of this study was to characterize the photophysical properties of 6AW in solutions of different pH, polarity, and environment and to ascertain its potential for biosynthetic incorporation into proteins. The majority of the reported studies were performed with the parent indole moiety, 6AI, to avoid complications in the photophysical studies arising from the zwitterionic side chain of 6AW. In water at pH 6, 6AW had an absorbance maximum of 325 nm, which was 45 nm to the red of the absorption maximum of a similar solution of tryptophan and 30 nm to the red of the absorption spectrum of 7AW (Figure 2a). The fluorescence spectrum of 6AW in the same buffer had an intense fluorescence maximum at 402 nm, compared to a fluorescence maximum of 340 nm for tryptophan and 400 nm for 7AW. Note the very weak fluorescence of 7AW under these conditions (Figure 2b). The absorbance and fluorescence spectra

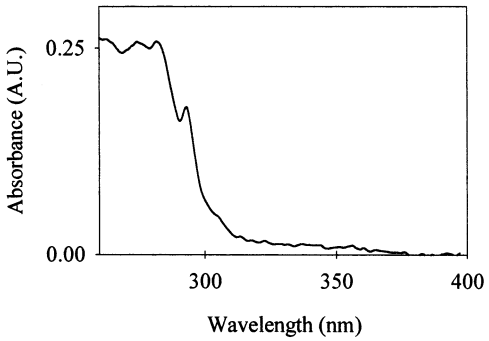

Figure 3. Absorbance spectrum of 6-azaindole in methylcyclohexane.

of 6AW and 6AI in water were similar (data not shown). The absorbance maximum of 6AI (320 nm) was at higher energy than that of 6AW, and the fluorescence maximum of 6AI was blue-shifted by 22 nm relative to that of 6AW to 380 nm.

By contrast, in methylcyclohexane, the absorbance spectrum of 6AI showed vibrational structure (Figure 3) with a noticeable shoulder at 293 nm and a maximum at 281 nm. The low-intensity tail of the spectrum extended beyond 300 nm. In chloroform, the absorbance spectrum showed a single broad band with a maximum at 290 nm (data not shown). No fluorescence from solutions of 6AI in either of these aprotic, nonpolar solvents could be detected regardless of excitation wavelength.

The absorbance spectra of 6AI in solutions at a selection of pH values are shown in Figure 4a. At pH 3, an absorbance maximum at 320 nm was observed. At pH 5 and above, the magnitude of this absorbance band decreased, until at pH 7 a shoulder became evident at 290 nm. At pH 8 and above, the absorbance maximum shifted to 290 nm, and at pH 10, there was negligible absorbance at wavelengths greater than 310 nm. The isosbestic point at 302 nm suggested that there were two species in equilibrium in the ground state. The fluorescence spectra of the same solutions are shown in Figure 4b. Maximal fluorescence intensity was observed at pH 3, with a spectral maximum of 380 nm. The magnitude of the fluorescence decreased with increasing pH, while the spectral maximum remained constant. Note that even at pH 10 there was appreciable fluorescence at 380 nm, although the spectral band appears to have broadened (vide infra).

The pH dependence of absorbance at 320 nm and fluorescence at 380 nm (excitation at 302 nm, the isosbestic point) are shown in Figure 4c. pK_a values of 8 and 7.2 were estimated from the absorbance and fluorescence data, respectively. The dependence of fluorescence intensity on pH showed that the fluorescence signal leveled off just above pH 8 and then again decreased just above pH 10. The data are consistent with a ground-state equilibrium between the protonated form of 6AI and a neutral form. The 320 nm absorption band may then be assigned to the protonated form, Pr, of 6AI (Figure 1). A NMR spectrum of 6AI in chloroform was fully consistent with a single species, the neutral N1 form. Hence, the absorbance band at 290 nm in chloroform, in methylcyclohexane, or in solutions at pH > 8 is assigned to the neutral form of 6AI.

The absorbance and fluorescence properties of 6AI in acetonitrile−aqueous mixtures were examined to determine its spectral behavior in a polar aprotic environment that might represent the interior of a protein. The absorbance and fluorescence properties of 6AI were examined in acetonitrile−water mixtures at different pH values. Solutions of 6AI in acetonitrile−water mixtures at pH 5 showed an absorbance spectrum that again included bands at 320 and 290 nm (data not shown). The fluorescence

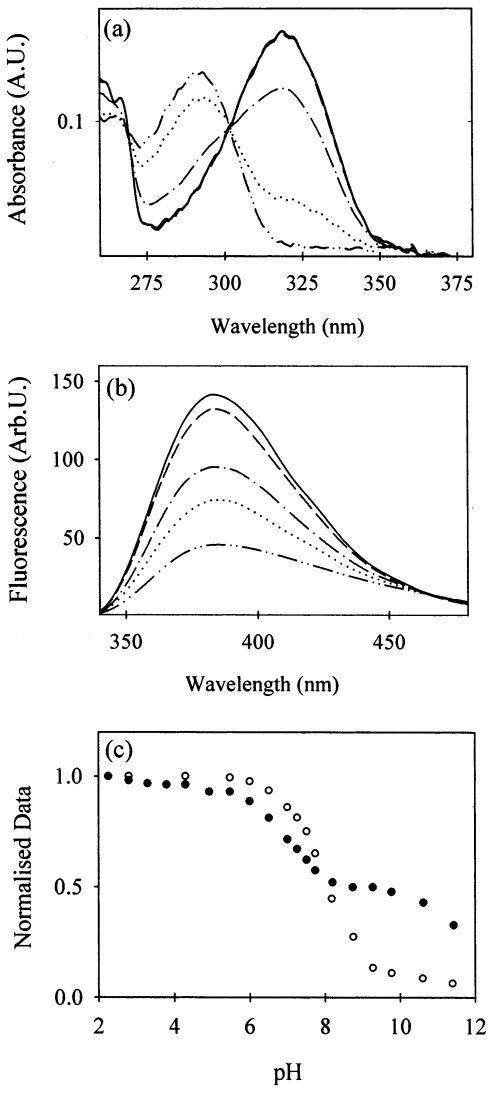

Figure 4. Absorbance and fluorescence spectra of 6AI in solutions of selected pH: (a) absorbance and (b) fluorescence of 2.5 μM solutions of 6AI at pH 3 (—), pH 5.0 (− − −), pH 7.5 (−•−), pH 9.0 (•••) and pH 10 (−••) and (c) change in absorbance at 320 nm (○) and fluorescence at 380 nm (●) of solutions of 2.5 μM 6AI. pK_a values of 7.2 and 8.0 were estimated for the fluorescence and absorbance data, respectively. For solutions at pH 3 and 5, a 10 mM citrate buffer was used. For solutions at pH 7, 10 mM sodium phosphate buffer was used, and for solutions at pH 9 and 10, 10 mM PIPES or TRIS buffers were used. Excitation wavelength was 302 nm in all cases.

spectra of the same solutions (data not shown) showed emission maxima at 380 nm in acetonitrile concentrations up to 90%. In 90% acetonitrile, pH 5, the emission maximum was slightly blue-shifted by 2 nm to 378 nm, and an increase in the fluorescence on the blue side of the spectrum was observed.

6AI in acetonitrile−water mixtures at pH 8 showed an absorbance band at 290 nm (Figure 5a) with a significantly smaller shoulder at 320 nm than that at pH 5. As in other mixed solvent experiments, the magnitude of the 320 nm absorbance decreased with increasing acetonitrile concentration. The fluorescence spectra of 6AI in acetonitrile, pH 8, mixtures of less than 50% acetonitrile showed fluorescence maxima at 380 nm, again with the magnitude decreasing with increasing acetonitrile concentration. However, in this set of experiments, even the fluorescence of the 25% acetonitrile, pH 8, solution showed spectral broadening. The normalized fluorescence spectra in Figure 5b show a small increase in fluorescence at the high-

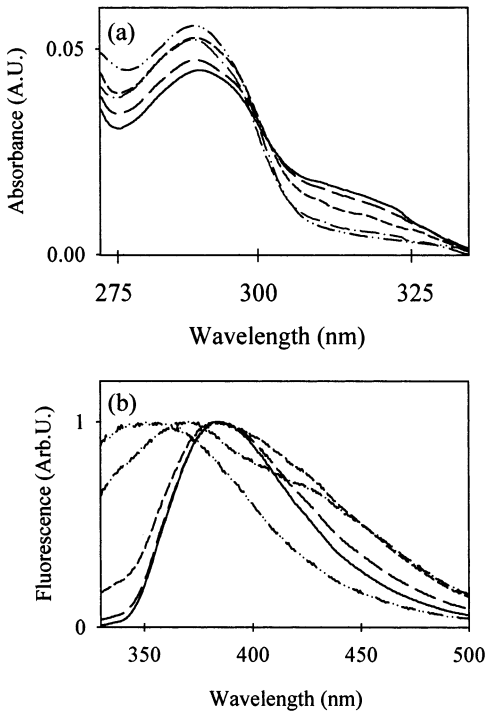

Figure 5. Absorbance and fluorescence spectra of 6AI in acetonitrile−water mixtures at pH 8: (a) absorbance and (b) fluorescence spectra of 2.5 μM solutions of 6AI in solutions of 9% (—), 25% (− − −), 50% (---), 75% (−•−) and 90% acetonitrile (−••) normalized to 1 at the fluorescence maximum.

energy edge of the 25% solution and a broadening on the low-energy side. In 75% acetonitrile, pH 8, the fluorescence spectra showed two maxima, one at 360 nm and another at 440 nm. In 95% acetonitrile, a single broad emission maximum was observed at 350 nm.

In acetonitrile−water mixtures at pH 10, the absorbance spectra showed a single band at 290 nm, which did not change with increasing acetonitrile concentrations (Figure 6a). There was negligible absorbance above 310 nm. The normalized spectra (Figure 6b) for this set of measurements were similar to those observed at pH 8. Spectral broadening was visible at all concentrations of acetonitrile, and 6AI in 90% acetonitrile, pH 10, had a single emission maximum at 340 nm and a smaller half-bandwidth than the same spectrum in the acetonitrile, pH 8, solution. In all of these different acetonitrile experiments, an isoemissive point was never observed.

The fluorescence spectra of 6AI in 75% and 90% acetonitrile,-pH 10, were normalized to have the same values on the high-energy side of the spectrum of the 90% solution. The normalized 90% solution spectrum was then subtracted from the normalized spectrum of the 75% solution, resulting in a difference spectrum with a maximum at 440 nm (Figure 6c). The data from these acetonitrile mixtures suggest that there are at least three species contributing to the fluorescence spectra of solutions having an important concentration of acetonitrile. One is the previously observed fluorescence at 380 nm. In addition, species with fluorescence maxima near 350 and 440 nm were observed.

The absorbance and fluorescence properties of 6AI in methanol−water mixtures were examined to determine the photophysical behavior of 6AI in a protic environment that was less polar than water. The absorption spectra of 6AI in unbuffered methanol−water mixtures showed a similar solvent dependency as that observed in acetonitrile−aqueous solutions (Figure 7a). In low concentrations of methanol, the absorbance was entirely due to the 320 nm band. The magnitude of the

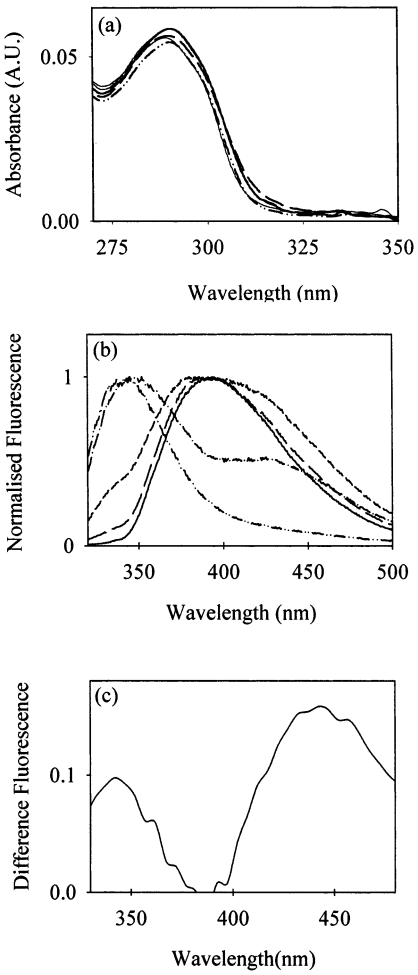

Figure 6. Absorbance and fluorescence spectra of 6AI in acetonitrile−water mixtures at pH 10: (a) absorbance and (b) fluorescence emission spectra of 2.5 μM solutions of 6AI in solutions of 9% (—), 25% (− − −), 50% (---), 75% (−•−) and 90% acetonitrile (−••) normalized to 1 at the fluorescence maximum. In panel c, spectra of 6AI in 9% and 90% acetonitrile were normalized at the blue edge of the spectrum and the normalized 9% spectrum was subtracted from 90% spectrum to give the resulting difference spectrum.

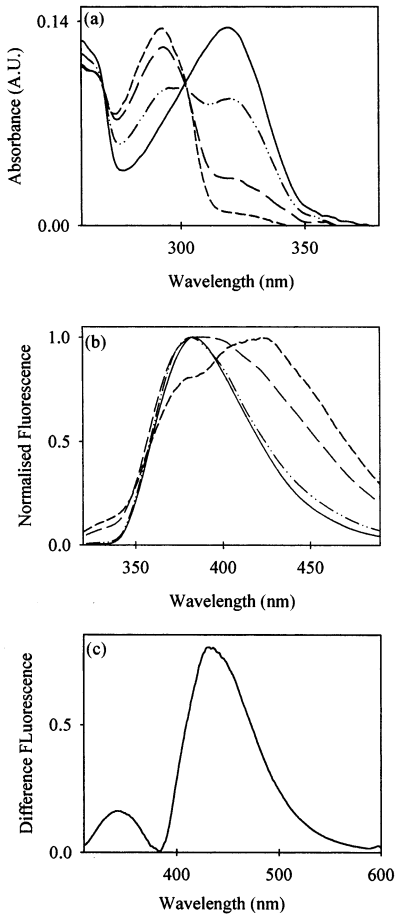

Figure 7. Absorbance and fluorescence spectra of 6AI in methanol−water mixtures: (a) absorbance and (b) normalized fluorescence emission spectra of 2.5 μM solutions of 6AI in 9% (—), 50% (−••), 90% (− − −) and 100% (---) methanol. In panel c, fluorescence spectra of 6AI in 9% and 100% methanol were normalized along the blue edge of the spectra and the 9% spectrum was subtracted from the 100% spectrum to give the resulting difference spectrum.

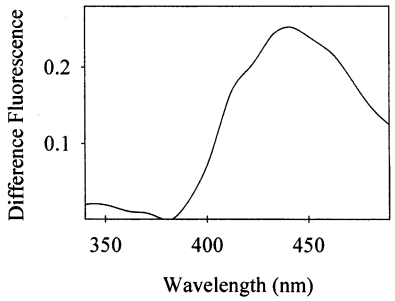

Figure 8. Fluorescence difference spectrum. Fluorescence spectra of 6AI at pH 5 and 10 were normalized along the blue edge. The pH 5 spectrum was then subtracted from the pH 10 spectrum to give the resulting difference spectrum.

absorbance at 320 nm decreased with increasing methanol concentration, and the absorbance maximum shifted to 290 nm. In 90% methanol, however, a distinct absorbance shoulder was still visible at 320 nm. This behavior is similar to that in acetonitrile−water mixtures in which the two ground-state species were N1 and Pr. The corresponding fluorescence spectra (Figure 7b) showed an emission maximum of 380 nm in 9% methanol−water. As the concentration of methanol increased, the magnitude of the 380 nm fluorescence decreased and a spectral broadening was observed. In the 100% methanol solution, the fluorescence of 6AI (Figure 7b) appeared to be complex, two fluorescence bands being present. Normalization of the aqueous pH 3 spectrum and the methanol spectrum of 6AI at 380 nm, followed by subtraction of the former from the latter, showed, as in comparable acetonitrile spectra, a clear fluorescence band at 440 nm (Figure 7c). In addition, there appeared to be a small amount of a fluorescence signal near 350 nm.

Normalization of the fluorescence spectra of 6AI in pH 3 and pH 10 buffers showed that the pH 10 spectrum showed broadening on the low-energy side. The normalized pH 3 spectrum was subtracted from the corresponding pH 10 spectrum, resulting in Figure 8. This figure shows a fluorescence maximum at 440 nm, but there also appears to be some residual signal at low wavelengths near 350 nm. The structural assignment of the 440 nm species was further investigated by studying the fluorescence properties of 6AI at high pH and in the presence of high concentrations of salts that are considered to be either proton donors or acceptors.

A single absorbance band was observed at 290 nm for solutions of 6AI at pH 10 with increasing concentrations of sodium carbonate, solutions in which the CO_3^{-2} ion is a strong conjugate base. The fluorescence spectra of the 0.1 M CO_3^{-2} solution (Figure 9) showed a 63% decrease in fluorescence intensity at 380 nm compared to the CO_3^{-2} free solution and a

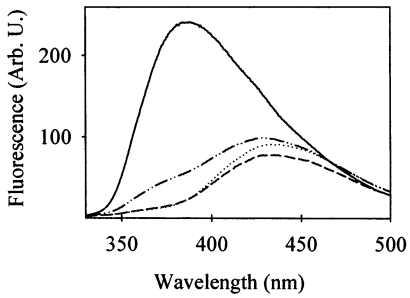

Figure 9. Fluorescence spectra of 6AI at pH 10 with sodium carbonate: fluorescence spectra of 2.5 μM solutions of 6AI at pH 10 with 0 M (—), 0.1 M (—••), 0.5 M (— — —) and 0.8 M (•••) sodium carbonate in 100 mM TRIS.

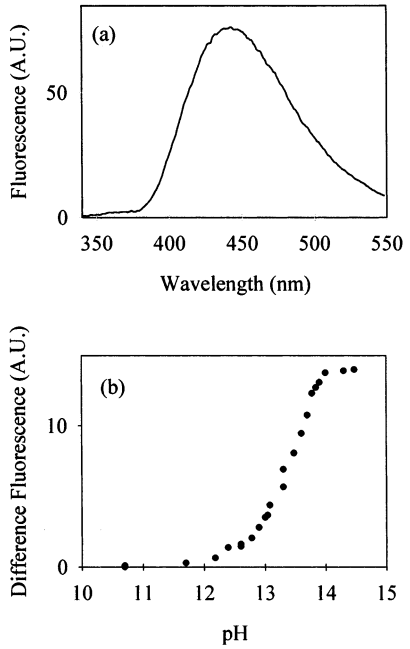

Figure 10. Fluorescence spectrum of 6AI in sodium hydroxide: (a) fluorescence spectrum of 2.5 μM 6AI in 1 M sodium hydroxide; (b) pH dependence of 6AI fluorescence measured at 440 nm.

shift in the emission maxima to 440 nm. Solutions of 0.5 and 0.8 M Na_2CO_3 resulted in a further intensity decrease of the fluorescence shoulder at 380 nm with the 440 nm band clearly dominating the spectrum.

At pH 14 (1 M NaOH), the absorption spectrum showed a single band with a maximum at 290 nm. The fluorescence of this solution showed a single broad fluorescence band with an emission maximum at 440 nm (Figure 10a). It was possible to examine the fluorescence of 6AI in solutions having pH values between pH 10 and 16. The magnitude of the fluorescence at 440 nm increased steadily with a concomitant loss of fluorescence intensity at 380 nm. No significant fluorescence was observed in the 380 nm region at pH 16. The pH dependence of the fluorescence signal at 440 nm between pH 10 and 16 is shown in Figure 10b, and an excited-state pK_a of 13.2 for this acid−base titration can be estimated.

The fluorescence quantum yields of 6AI were measured at pH 5, 7.4, 10, and 14 and in methanol and are shown in Table 1. All measurements were performed with 302 nm excitation. The quantum yield was found to be highly pH-dependent. At pH 14 and above, the emission maximum shifted to 440 nm and the quantum yield was found to be 0.15. At pH 5, the quantum yield is 0.55. In methanol, the value is the net quantum yield of two different spectral species emitting at 380 and 440 nm.

TABLE 1: Spectral Maxima and Fluorescence Quantum Yields of 6-Azaindole in Different Solvent Conditions

solvent	λ_{max} (nm)	ϕ (20 °C)[a]
buffer, pH 5	380	0.55 ± 0.02
buffer, pH 7.4	380	0.29 ± 0.01
buffer pH 10	380	0.27 ± 0.01
NaOH, pH 14	440	0.15 ± 0.01
methanol	380	0.30 ± 0.03[b]

[a] Determined at 20 °C with a band-pass of 5 nm using POPOP in cyclohexane as a standard. [b] Corrected for the refractive index of methanol

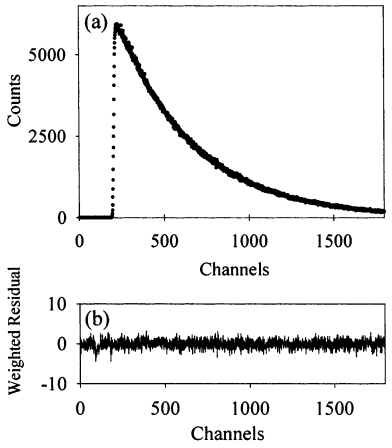

Figure 11. Fluorescence decay curve for 6AI: (a) 2.5 μM 6AI in 10 mM citrate buffer, pH 5 at 20 °C. Excitation and emission wavelengths were 302 and 380 nm, respectively, with bandwidths of 10 nm. Decay data were collected into 2000 channels with a timing calibration of 0.2 ns/channel. Data were fit to a single-exponential decay curve with τ = 10.9 ns. Panel b shows the weighted residual plot of the best fit for the sample with χ^2 = 1.02.

The fluorescence intensity decay of 6AI at pH 5 displayed single-exponential decay kinetics at all emission wavelengths with τ = 10.9 ns (sample data shown in Figure 11). At pH 10, the decay kinetics were no longer well-described by a single-exponential model but required two or three exponential terms to fit the data adequately at different fluorescence wavelengths. Global analysis of the decay kinetics at pH 10 was not able to fit the data at all wavelengths to a single decay model. Rather, separate global analyses were performed on data sets between 360−420 and 465−500 nm (Table 2). The global analysis of decay data between 360 and 420 nm gave a satisfactory fit to a double-exponential decay model with lifetimes of 0.33 and 8.38 ns with positive preexponential terms. At the single wavelength 450 nm, the decay kinetics gave a good fit to a double-exponential decay with decay times of 9 and 5.8 ns. At wavelengths greater than 460 nm, the decay kinetics fit well to a triple-exponential model with decay times of 0.33, 9.0, and 5.8 ns. The preexponential term associated with the 0.33 ns component was negative at emission wavelengths greater than 465 nm, characteristic of an excited-state reaction.

6AW was biosynthetically incorporated into a single-tryptophan mutant of rat calmodulin (Y99W). The level of analogue incorporation, estimated by amino acid analysis, was found to be 80% (G. Abbott, personal communication). The absorbance spectra of Y99(6AW) at pH 7.4 (Figure 12a) showed an absorbance maximum at 281 nm with a shoulder at 292 nm. This shoulder extended to greater than 310 nm, albeit at low intensity.

TABLE 2: Global Analyses Results for the Fluorescence Decay Kinetics of 6-Azaindole in pH 10 Buffer[a]

wavelength (nm)	τ_1[b] (ns)	α_1[c]	τ_2 (ns)	α_2[c]	τ_3 (ns)	α_3[c]
360	0.33	0.41	8.38	0.59		
380	0.33	0.32	8.38	0.68		
400	0.33	0.30	8.38	0.70		
420	0.33	0.31	8.38	0.69		
450			9.11	0.43	5.90	0.57
465	0.33	−0.16	9.05	0.45	5.80	0.71
480	0.33	−0.21	9.05	0.41	5.80	0.80
490	0.33	−0.28	9.05	0.40	5.80	0.88
500	0.33	−0.29	9.05	0.38	5.80	0.92

[a] Two separate global analyses were conducted. Data from 360 to 420 nm fit to two exponentials, while data from 460 to 500 nm fit to three exponentials. Data at 450 nm was fit as an individual data set. Excitation was at 302 nm. Standard error on decay times was ±0.01 ns. Average κ^2 was 1.1. [b] In global analysis, the short decay time was fixed on the basis of the fact that individual wavelengths had a 330 ps component. [c] Preexponentials were normalized.

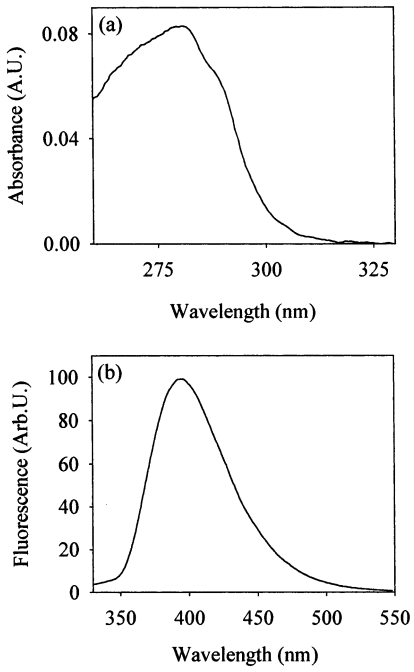

Figure 12. Absorbance and fluorescence of calmodulin Y99(6AW): (a) absorbance and (b) fluorescence spectrum of 1 μM Y99(6AW) in 10 mM HEPES, 100 mM KCl, pH 7.4. Excitation wavelength was 308 nm.

The fluorescence of the same solution is shown in Figure 12b with maximal fluorescence intensity observed at 395 nm.

Discussion

The different structural forms of 6AI are shown in Figure 1. The NMR spectrum of 6AI in chloroform was clearly consistent with the structure of the neutral N1 species and hence is identified with the 290 nm absorption band. The absorbance spectral behavior at different pH values is best described by the ground-state equilibrium shown in eq 1.

$$N1^* + H^+ \rightleftarrows Pr^* \quad (1)$$

The pK_a of this equilibrium as determined from the absorbance data was found to be 8. This pK_a is best assigned as being due to the protonation of N_6 of the indole ring in which both ring nitrogens bear a proton. An alternate ground-state equilibrium might be deprotonation of the N_1−H to form an anion. However, by analogy with indole, this pK_a is likely to exceed a value of 16.[22] The 320 nm absorbance band, observed at acidic pH, was therefore assigned to the N_6 protonated species, Pr, and is dominant at pH 5 and gives rise to the 380 nm fluorescence spectral maximum at this pH. The singlet excited-state decay time of Pr was 10.8 ns. At pH 10 and above, the amount of ground-state Pr will be negligible; thus, the predominant absorbance band at 290 nm is due to N1. Yet at all pH values between 3 and 10, the fluorescence maximum remains constant at 380 nm. Only the intensity value appeared to change (λ_{ex} = 302 nm). However, careful examination of the difference spectra in pH 10 and in methanol solutions (Figures 8 and 7c, respectively) revealed a very weak signal at 350 nm. This weak fluorescence signal at 350 nm is suggested to originate from the neutral N1* species, the spectral region where the fluorescence of the indole nucleus in aqueous solution is normally observed. At this time, the nature of the efficient quenching processes in N1* are not understood. Note that a very weak fluorescence band in 95% acetonitrile solutions was observable. It is significant that the pK_a values estimated from absorbance and fluorescence experiments differ by 0.8 units, that from fluorescence being 7.2. Indeed in the fluorescence pH titration, the observed intensity curve at first leveled off between pH 8 and 10 and then declined further at higher pH values. The sum of these observations strongly suggests that there is an excited-state reaction occurring when N1 is excited, forming Pr* even at high pH at which there is negligible proton concentration. It is suggested that in aqueous solution in which the concentration of the ground-state Pr is minimal there is an excited-state proton-transfer event in which N1* abstracts a proton from the solvent, water, to form Pr* and the conjugate base, OH^-. Using the Förster cycle[23] based on the differences in 0−0 energy values from the absorption spectra and a ground-state pK_a = 8, we calculated an excited-state pK_a of 14.7 for the N1* to Pr* equilibrium. The 0−0 energy was taken as the wavelength that had 10% of the intensity of the spectral maximum on the low-energy side of the respective spectra. An increase in pK_a of 7 units between the ground and excited state indicates that N1 becomes much more basic in the excited state and is highly likely to abstract a proton from a proton source such as water.

From the absorbance spectra shown in Figures 4a, 5a, 6a, and 7a, it was clear that the ground-state equilibrium between Pr and N1 also exists in both acetonitrile−water and methanol−water mixtures. In all cases, an isosbestic point at 302 nm was observed, consistent with N1 and Pr being the predominant ground-state species. It is significant that the fluorescence spectra of 6AI in all acetonitrile−buffer mixtures showed no isoemissive point indicating the presence of more than two fluorescent species. The normalized fluorescence spectra, Figures 5b, 6b, and 7b, are particularly informative. In pH 8 and 10 acetonitrile−water solutions at high acetonitrile concentrations, the fluorescence has low intensity with a clear maximum at 340 nm. In greater than 80% acetonitrile−water, the absorbance spectra show N1 to be the predominant ground-state species, as observed in solutions of alkaline pH. In 100% acetonitrile, 6AI was nonfluorescent. The reason for this behavior is not understood. At intermediate acetonitrile concentrations, a broadening on both sides of the fluorescence spectra was seen, and in 75% acetonitrile−water solutions at pH 8 and 10, a broad shoulder at wavelengths longer than 400 nm emerged.

In methanol−water solutions, the fluorescence was largely that of Pr* until high concentrations of methanol were used, and then the spectra showed a marked broadening on the low-energy side of the spectra. In 100% methanol, the spectrum and

the difference spectrum (Figure 7b,c) are fully consistent with the total spectrum including fluorescence from Pr*, another species with a fluorescence maximum at 440 nm having a modest intensity, and perhaps a very weak fluorescence near 350 nm. By analogy with the 95% acetonitrile fluorescence spectrum, the 350 nm emission may be assigned to very weak fluorescence from N1*. In methanol, the predominant ground-state species would be N1, and thus, the observation of Pr* fluorescence requires that N1* abstracts a proton from methanol to form Pr* and the methoxide anion (MeO^-). The assignment of the third species having fluorescence at 440 nm at pH 14, as well as the fluorescence maximum at 440 nm in the acetonitrile (pH 10, 95%) and methanol difference spectra (Figures 6c and 7c), to a 6AI structure is required for a full photophysical rationalization of the excited-state behavior of 6AI.

The 440 nm species must be the result of another excited-state process. There are two candidates, the anion form of 6AI, AN, or the tautomeric form N6 (Figure 1). It is important that even in aqueous pH 10 solution fluorescence from a 440 nm species was observed. At this pH, the concentration of hydroxide anion is 10^{-4} M making it unlikely that AN* would form from N1* at this pH. The 440 nm fluorescence is assigned to that from N6* formed according to the following scheme (eq 2).

In solution conditions in which N1 can be the only ground-state species such as at pH 10 or in methanol, the first step in the process is excitation of N1 to form N1*

$$\mathrm{N1} + h\nu \rightarrow \mathrm{N1^*} \tag{2}$$

Fluorescence from N1* is predicted to be near 350 nm in a polar environment and in this work is only clearly observed in 90% acetonitrile−water solutions. It is proposed that the next step is excited-state proton abstraction from the protic solvent methanol or water to form Pr* and the alkoxide, RO^-

$$\mathrm{N1^* + ROH \rightarrow Pr^* + RO^-}$$
$$\mathrm{R = CH_3 \text{ or } H} \tag{3}$$

This results in the fluorescence observed at 380 nm. It is proposed that in pure water or methanol the conjugate base, RO^-, formed during the excited-state reaction (eq 3) is retained in the solvent cage during the lifetime of Pr* and acts as the proton acceptor, abstracting the N_1−H proton to form the excited-state tautomer, N6*, which is the origin of the 440 nm fluorescence.

$$\mathrm{Pr^* + RO^- \rightarrow N6^* + ROH} \tag{4}$$

Thus in the excited state, the N1* is a stronger acid than N6*. The experiments with cacodylate and carbonate buffers support this rationalization. In these cases, when the conjugate base of the buffer salt was present in high concentrations, no fluorescence was observed from Pr* and the only fluorescence observed was at 440 nm. Clearly the conjugate base was acting to abstract a proton from Pr*. The fluorescence titration behavior between pH 10 and 15 reflects the excited-state pK_a between Pr* and N6*, and pK_a* was estimated to be 13.2.

The excited-state decay behavior of 6AI at pH 10 can now be better understood. The excitation of N1 leading to N1* results in a series of reactions between different excited-state species owing to their pK_a differences from the corresponding species in the ground state. The short decay time component (0.33 ns) is assigned to the excited singlet state lifetime of N1*. The steady-state difference spectrum (Figure 8) revealed a very weak fluorescence near 350 nm, which we had earlier suggested was

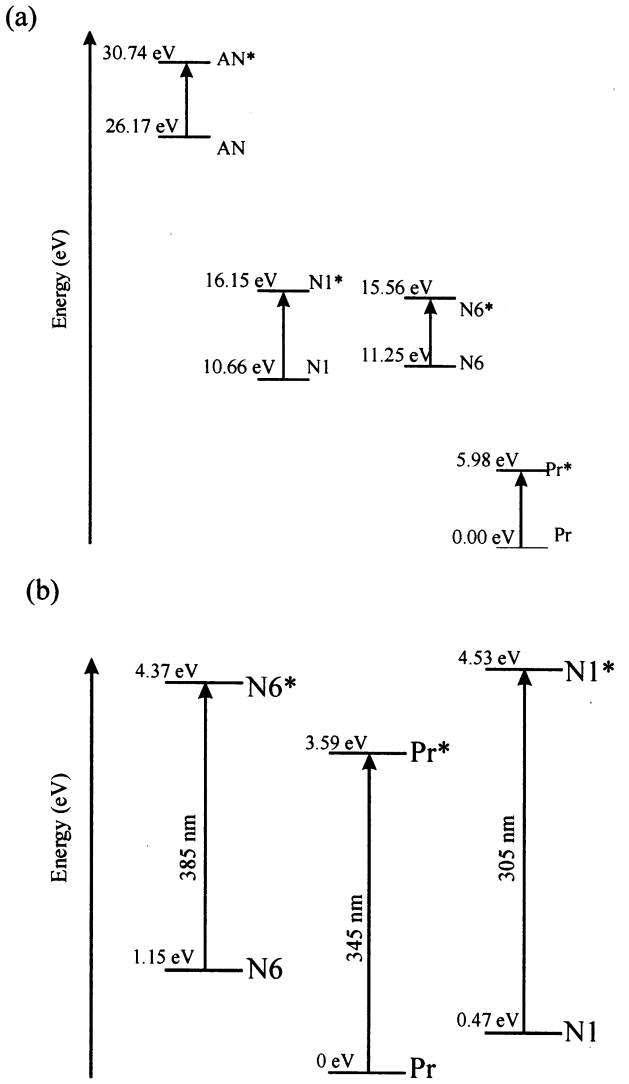

Figure 13. Relative energy levels of the ionic and tautomeric species of 6AI: (a) predicted energy levels from ab initio calculations in vacuo. Refer to methods section for details regarding the calculations. Panel b shows the relative energy levels of 6AI species determined from spectroscopic and pK_a values. The relative energy difference between each of the ground- and excited-state species was calculated from the fluorescence or absorbance spectra using the 0−0 band. The energy difference between Pr and N1 and Pr* and N1* were calculated from the pK_a values using the Arrhenius equation.

due to this species. At longer wavelengths (>450 nm), the preexponential associated with this component is negative, consistent with the formation and fluorescence of Pr*. The long decay time of 8.38 or 9.05 ns is assigned to this species. This decay time is slightly shorter than the value of Pr* at pH 5. This would be expected if there were another excited-state reaction such as that leading to N6*. The 5.81 ns decay time is thus assigned to this latter species. The kinetic scheme does not require that the 0.33 ns component actually be observable at long wavelengths, rather at these wavelengths, this component is associated with the decay kinetic expression for Pr*. On the other hand, the 5.81 ns component is not observed at short wavelengths because it does not contribute to the kinetic behavior of the short wavelength species.

Ab initio calculations of 6AI in vacuo provided estimates of the relative energies of these species, and Figure 13 depicts these relationships. This chart was useful in directing our experiments and rationalization of the spectroscopic assignments. The

TABLE 3: ZINDO Calculations Using the ab Initio Excited State Geometries

species	predicted emission (nm)	actual emission (nm)
Pr	364	380
N1	308	340
N6	467	440
AN	371	*a*

[a] Fluorescence from AN was not observed

TABLE 4: Energy Difference between the Different 6AI Species[a]

	species[b]					
	Pr	N6	N1	Pr*	N6*	N1*
Pr	0.00	1.15	0.47	3.59	4.37	4.53
N6	−1.15	0.00	−0.68	−2.44	3.22	4.28
N1	−0.47	0.68	0.00	3.12	3.90	4.06

[a] From pK_a determination and spectral positions. [b] Relative energy difference between species measured in electronvolts (eV).

predicted energies of AN and AN* strongly indicated that it was unlikely that the 440 nm species could be assigned to AN* fluorescence, and there was no excited-state process involving this species that was likely to be playing a role in the reaction scheme. On the other hand, the scheme properly shows that excitation of N1* can lead to Pr* or even N6*. ZINDO calculations using the ab initio excited-state geometries predicted the emission maxima of the different species (Table 3), and the differences between these calculated maxima and those observed are noted. These differences are not surprising because in vacuo calculations were performed.

It is now possible to propose a chart that relates the relative energies of the several species involved in the different ground-state and excited proton-transfer processes. The relative energies of the ground-state species and each of their respective excited singlet states were estimated in the following manner. For N1 and Pr, the 0−0 energy was taken as the energy at the point on the low-energy side of their respective absorption spectra that was 10% of the maximum intensity. For N6, the 0−0 energy was taken as the energy value on the high-energy side of its fluorescence spectrum that was 10% of the intensity maximum. These values are summarized in Table 4. The measured pK_a (8) of the Pr to N1 equilibrium permits the calculation of the free energy difference between these species. The pK_a* (13.2) of the excited-state equilibrium between Pr* and N6* was determined from the alkali titration experiment using the Arrhenius relationship. The free energy differences between these two equilibria allow the assignment of the relative energies of each of the six species (Table 4). The chart shows the central role of Pr and Pr* in the interconversion between N1 and N6 in both the ground and excited state. The excited-state tautomerization between N1* and N6* must proceed via Pr*. These relative energies are fully consistent with the rationalization of the species assignment and the excited-state processes proposed above.

The rationalization of the photophysics of 6AI provides the key components for interpreting the fluorescence behavior of biosynthetically incorporated 6AW in proteins. In CaM Y99-(6AW), there was negligible absorbance of 6AW at 325 nm, yet a relatively weak fluorescence at 395 nm was observed. On the basis of the photophysical properties reported in this work, the 6AW in the CaM exists as the neutral form in the protein and is able to undergo some of the same excited-state proton-transfer reactions that were observed in the solution studies of 6AW. The photophysical properties of 6AI potentially offer increased information content to study the interactions of proteins in their complexes with other biomolecules, especially because the fluorescence behavior will be very sensitive to exposure to an aqueous environment.

Acknowledgment. The authors gratefully acknowledge J. B. Alexander Ross and William Laws for allowing the fluorescence decay data to be collected using their instrument. The authors thank Madeline Shea for the generous gift of the rCaM plasmid DNA construct and Dmittri Goussev for performing the NMR experiment. This work was funded by a Discovery Grant from NSERC (Natural Sciences and Engineering Research Council, Canada) to A.G.S. and in part by NIH (Grant GM42588) to R.S.P.. Lise Murphy was a student working at WLU under the RISE program.

References and Notes

(1) Royer, C. A. *Methods Mol. Biol.* **1995**, *40*, 65.

(2) Eftink, M. R. *Methods Biochem. Anal.* **1990**, *35*, 117.

(3) Szabo, A. G. In *The Enzyme Catalysis Process*; Cooper, A., Houben, J. L., Chien, L. C., Eds.; NATO ASI Series A, Life sciences, Vol. 178; Plenum Publishing: New York, 1989; p 123.

(4) Hogue, C. W. V.; Rasquinha, I.; Szabo, A. G.; MacManus, J. P. *FEBS Lett.* **1992**, *310*, 269.

(5) Ross, J. B. A.; Senear, D. F.; Waxman, E.; Kobi, B. B.; Rusinova, E.; Huang, Y. T.; Laws, W. R.; Hasselbacher, C. A. *Proc. Natl. Acad. Sci. U.S.A.* **1992**, *89*, 12013.

(6) Ross, J. B. A.; Szabo, A. G.; Hogue, C. W. V. *Methods Enzymol.* **1997**, *273*, 151.

(7) Twine, S. M.; Szabo, A. G. *Methods Enzymol.*, in press.

(8) Gore, M. G. In *Spectrophotometry & Spectrofluorimetry: A Practical Approach*; Gore, M. G., Ed.; Oxford University Press: New York, 2000; p 242.

(9) Sloan, M. J.; Phillips, R. S. *Bioorg. Med. Chem. Lett.* **1992**, *2*, 1053.

(10) Drapeau, G. R.; Brammar, W. J; Yanofsky, C. *J. Mol. Biol.* **1968**, *35*, 357.

(11) Sambrook, J.; Fritsch, E. F.; Maniatis, Y. *Molecular Cloning: A Laboratory Manual*, 2nd ed.; Cold Spring Harbour Laboratory Press: Cold Spring Harbor, NY, 1989; p A3.

(12) Putkey, J. A.; Slaughter, G. R.; Means, A. R. *J. Biol. Chem.* **1985**, *260*, 4704.

(13) Dahms, T. E. S.; Willis, K. J.; Szabo, A. G. *J. Am. Chem. Soc.* **1995**, *117*, 2321.

(14) Hasselbacher, C. A.; Schartzw, G. P.; Glass, J. D.; Laws, W. R. *Int. J. Pept. Protein Res.* **1991**, *38*, 459.

(15) Willis, K. J.; Szabo, A. G. *Biochemistry* **1989**, *28*, 4902.

(16) Grinvald, A.; Steinberg, I. Z. *Anal. Biochem.* **1974**, *59*, 583.

(17) Beechem, J. M.; Knutson, J. R.; Ross, J. B. A.; Turner, B.; Brand, L. *Biochemistry* **1983**, *22*, 6054.

(18) Knutson, J. R.; Beechem, J. M.; Brand, L. *Chem. Phys. Lett.* **1983**, *102*, 501.

(19) Frisch, M. J.; Trucks, G. W.; Schlegel, H. B.; Scuseria, G. E.; Robb, M. A.; Cheeseman, J. R.; Zakrzewski, V. G.; Montgomery, J. A., Jr.; Stratmann, R. E.; Burant, J. C.; Dapprich, S.; Millam, J. M.; Daniels, A. D.; Kudin, K. N.; Strain, M. C.; Farkas, O.; Tomasi, J.; Barone, V.; Cossi, M.; Cammi, R.; Mennucci, B.; Pomelli, C.; Adamo, C.; Clifford, S.; Ochterski, J.; Petersson, G. A.; Ayala, P. Y.; Cui, Q.; Morokuma, K.; Malick, D. K.; Rabuck, A. D.; Raghavachari, K.; Foresman, J. B.; Cioslowski, J.; Ortiz, J. V.; Stefanov, B. B.; Liu, G.; Liashenko, A.; Piskorz, P.; Komaromi, I.; Gomperts, R.; Martin, R. L.; Fox, D. J.; Keith, T.; Al-Laham, M. A.; Peng, C. Y.; Nanayakkara, A.; Gonzalez, C.; Challacombe, M.; Gill, P. M. W.; Johnson, B. G.; Chen, W.; Wong, M. W.; Andres, J. L.; Head-Gordon, M.; Replogle, E. S.; Pople, J. A. *Gaussian 98*, revision A.6; Gaussian, Inc.: Pittsburgh, PA, 1998.

(20) Podolyan, V.; Gorb, L.; Leszczynski, J. *J. Phys. Chem A* **2000**, *104*, 7346.

(21) Gordon, M. S. Hydrogen transfer in 7-azaindole. *J. Phys. Chem.* **1996**, *100*, 3974.

(22) Szabo, A. G. In *Proceedings of a NATO Advanced Study Institute on Time-Resolved Fluorescence Spectroscopy in Biology and Biochemistry*; Cundall, R. B., Dale, R. E., Eds.; Plenum Press: New York, 1980; p 621.

(23) Parker, C. A. *Photoluminescence of Solutions*; Elsevier Publishing: Essex, England, 1968; p 333.